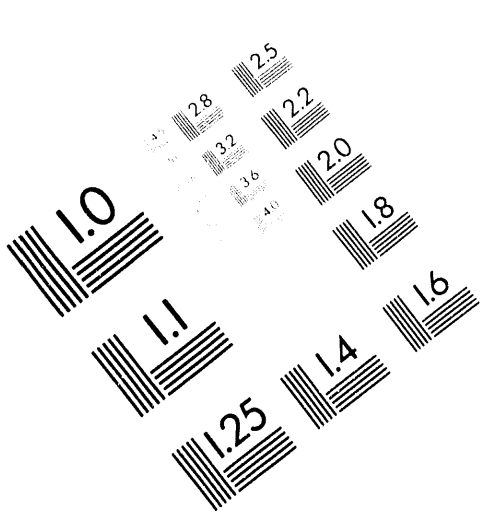

Association for Information and Image Management

1100 Wayne Avenue, Suite 1100
Silver Spring, Maryland 20910

301/587-8202

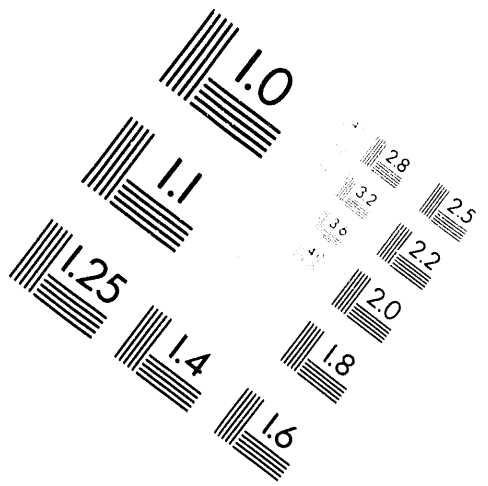

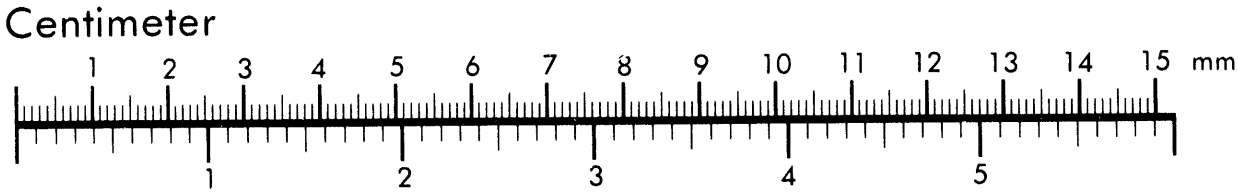

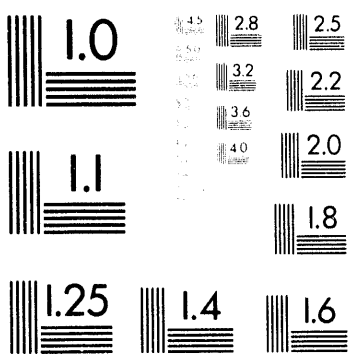

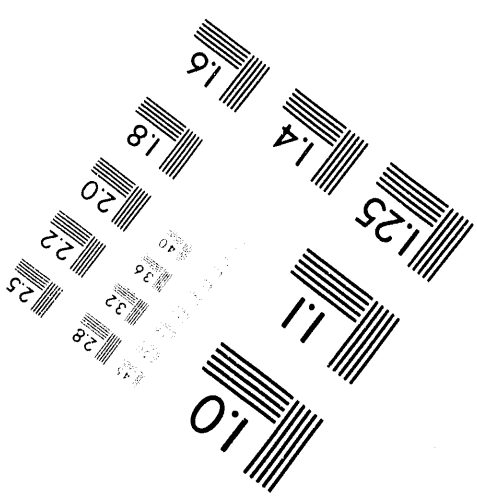

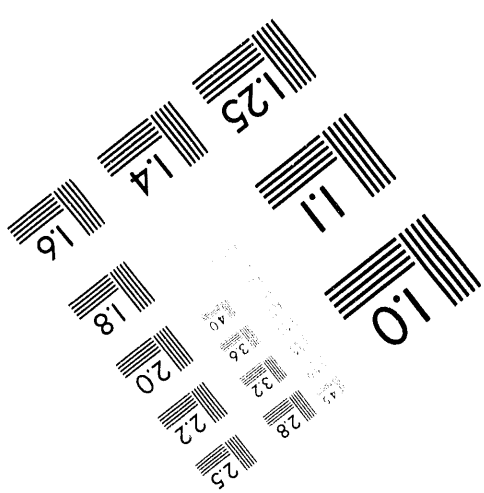

MANUFACTURED TO AIIM STANDARDS
BY APPLIED IMAGE, INC.

1 of 1

2.

Conf-940838--5

Finite–Rate Chemistry and Transient Effects in Direct Numerical Simulations of Turbulent Non–premixed Flames

SHANKAR MAHALINGAM

Center for Combustion Research

Department of Mechanical Engineering

University of Colorado, Boulder, CO 80309-0427, USA

JACQUELINE H. CHEN

Combustion Research Facility

Sandia National Laboratories , Livermore CA 94551, USA

LUC VERVISCH

Laboratoire de Mécanique des Fluides Numériques

INSA-Rouen, CORIA, URA-CNRS-230, France

Corresponding Author:

Jacqueline H. Chen
Combustion Research Facility
Sandia National Laboratories
Livermore, CA 94551, USA
Tele: (510) 294 2586
FAX: (510) 294 1004
e-mail: jhchen@california.sandia.gov

Word Length:

Text: 3068, Equations: 3×21 = 63, Figures: 11×200 = 2200
Total word count: 5331

Preferred Presentation Mode:

Oral presentation

Preferred Publication:

Combustion and Flame

Generic Approach:

B - Numerical Modeling

Subject Matter:

(3.0) - Flames
(3.7) - Transition and Turbulent Flames (Diffusion)
(3.9) - Direct Numerical Simulation

Finite–Rate Chemistry and Transient Effects in Direct Numerical Simulations of Turbulent Non–premixed Flames

SHANKAR MAHALINGAM

Center for Combustion Research

Department of Mechanical Engineering

University of Colorado, Boulder, CO 80309-0427, USA

JACQUELINE H. CHEN

Combustion Research Facility

Sandia National Laboratories , Livermore CA 94551, USA

LUC VERVISCH

Laboratoire de Mécanique des Fluides Numériques

INSA-Rouen, CORIA, URA-CNRS-230, France

Abstract

Three-dimensional Direct Numerical Simulations (DNS) of turbulent non-premixed flames including finite-rate chemistry and heat release effects were performed. Two chemical reaction models were considered: 1) a single–step global reaction model in which the heat release and activation energy parameters are chosen to model methane–air combustion, and 2) a two–step reaction model to simulate radical production and consumption and to compare against the single–step model. The model problem consists of the interaction between an initially unstrained laminar diffusion flame and a three-dimensional field of homogeneous turbulence. Conditions ranging from fast chemistry to the pure mixing limit were studied by varying a global Damköhler number. Results suggest that turbulence–induced mixing acting along the stochiometric line leads to a strong modification of the inner structure of the turbulent flame compared with a laminar strained flame, resulting in intermediate species concentrations well above the laminar prediction. This result is consistent with experimental observations. Comparison of the response of the turbulent flame structure due to changes in the scalar dissipation rate with a steady strained laminar flame reveals that unsteady strain rates experienced by the turbulent flame may be responsible for the observed high concentrations of reaction intermediates.

Introduction

Turbulent flames are intrinsically difficult to model due to the strong coupling that exists between the chemical heat release and the fine scale turbulent motion. Non-premixed flames are characterized by their internal structure and by the transport of fuel and oxidizer to the reaction zone where products of combustion are formed. In the fast chemistry limit, where the rate of chemical reaction is governed by the rate of mixing of scalars, the assumption of equal molecular diffusivity between species allows a direct link between the instantaneous reaction rate and the dissipation rate of a conserved scalar [1]. However, important physical effects such as extinction and pollutant formation can be successfully modelled only if finite-rate chemical effects are taken into consideration. Finite-rate effects govern the inner structure of these flames where regimes far from equilibrium are observed.

Within this framework, the laminar flamelet approach is attractive, since it provides an effective method by which detailed chemistry can be combined with turbulent simulations. In the standard flamelet approach, the mixture fraction (Z) and scalar dissipation rate (χ) are sufficient to determine the local instantaneous thermochemical state in the turbulent flow. One limitation of this approach is that standard flamelet libraries are composed of steady strained laminar flames. Experimental data [2, 3, 4] suggest that the reaction zone structure of turbulent jet flames differ significantly from steady strained laminar flames. For instance, measurements show elevated intermediate species concentrations as compared to predictions from steady strained laminar flame calculations. Maußet al. [5] and Barlow and Chen [6] identified certain unsteady strain rate histories in laminar flame calculations that can contribute to elevations in CO and OH mass fractions measured in flames. Haworth et al. [7] presented a simple correction to the stretched laminar flamelet model to account for flame response to unsteady strain effects.

A significant role of direct numerical simulations (DNS) of turbulent combustion is to assess the importance of various physical mechanisms such as transient, differential diffusion, heat release, and curvature effects. In DNS, all of the relevant flow and reactive scales are solved and, therefore, no closure model is needed for the small scale mixing and chemical reaction. Both scalar and vector fields of interest to combustion modelers are attainable from post–processing the numerical databases. Using this approach, differential diffusion and finite–rate chemistry effects in turbulent non-premixed flames have been studied [8, 9, 10] with single–step and two–step chemical reaction models. In the present paper flame structure data obtained from DNS of turbulent non–premixed

flames modeled with single- and two-step chemical kinetics models is examined and compared with predictions from a steady laminar flame established in a Tsuji burner configuration. Although several mechanisms could potentially contribute to the experimentally observed higher concentrations of intermediates as compared to steady laminar flame predictions [6], the emphasis in the present paper is on the role of transient effects.

Methodology

In the present DNS approach the compressible reacting Navier-Stokes, energy, and species equations are solved using an explicit higher-order Pade finite-difference method [11]. The problem investigated involves an initially one–dimensional laminar, unstrained, diffusion flame interacting with a three-dimensional field of isotropic decaying turbulence. Detailed descriptions of the flow field, numerical method, and nondimensionalization are presented in Chen et al. [8] and Vervisch [12]. Nonreflecting boundary conditions [13] are imposed in the direction normal to the initial laminar flame and periodic boundary conditions are prescribed in the other two directions.

Two different Arrhenius chemical kinetics models are investigated in this paper. In the single-step model ($A + B \rightarrow P$, Model 1), the overall heat release and activation energy parameters are representative of methane-air combustion. The rate of the global step is varied in order to investigate conditions that extend from strong (near–equilibrium) chemistry to weak (near–extinction) chemistry. In the two-step model ($A + B \rightarrow I, A + I \rightarrow P$, Model 2) a radical–like species I is produced and is subsequently consumed by the fuel species A. The second step proceeds with an activation energy four times smaller and an enthalpy of reaction five times larger than the first step. This model was chosen to investigate the effect of a fast–diffusing, radical–like species on flame topology, extinction dynamics, and the influence of turbulence on intermediate radical concentration. The stoichiometric coefficients are chosen such that the overall global step is identical to the single–step model; thus, the effects of multiple steps and differential diffusion could be evaluated. In order to isolate the effect of unsteadiness due to the turbulence, the Schmidt numbers of all of the species are taken to be unity, thereby eliminating the possibility of differential diffusion.

The turbulence field is prescribed by an initial turbulent kinetic energy spectrum

$$E(k) = C_0 \frac{u_0^2}{k_0} \left(\frac{k}{k_0}\right)^4 \exp\left[-2\left(\frac{k}{k_0}\right)^2\right], \tag{1}$$

where k is the wavenumber, k_0 is the wavenumber corresponding to the most energetic eddies, and

u_0 is the rms velocity. The initial Damköhler number,

$$Da = \frac{l_t}{u_0}\left[\frac{1}{\delta_{fl}}\int_{\delta_{fl}} \omega dx\right], \tag{2}$$

is defined as the ratio of the turbulent eddy turnover time to a characteristic chemical reaction time based on the heat release; l_t is the turbulent integral length scale and δ_{fl} the flame thickness based on the reaction rate ω appearing in the energy equation. The initial Taylor Reynolds number of the simulations is fifty, a value relevant for experimental jet flames [14]. The flame thickness is such that flame–turbulence interactions are limited to a range of reactive and turbulence scales of the same order of magnitude. These choices are well suited for studying the dynamics of extinction.

In order to compare data obtained from the DNS with steady laminar diffusion flame predictions, computations were made of the steady flame structure in a Tsuji burner configuration. The kinetic scheme and the corresponding parameters were chosen to be identical to those used in the DNS. The boundary layer model reduces the problem to a one– dimensional boundary value problem [15] which is solved with an algorithm that combines Newton's method and time–stepping in order to achieve convergence [16].

Global feature of the finite-rate chemistry effects

Figure 1 is an isosurface of the instantaneous reaction rate for Model 1 illustrating the effect of the turbulence on the flame after approximately two eddy turnover times. Note that the initially plane laminar flame has become stretched and distorted by the turbulence, and furthermore, pockets of extinction have formed in regions where the flame is unable to sustain the locally high tangential strain rates. Note that the flame in the present DNS is not sufficiently wrinkled for iso–stoichiometric scalar surface interactions which potentially could lead to self–annihilation through a dissipative process. The effect of the flame on the turbulence is shown in Fig. 2. Note that vorticity is unable to penetrate the flame in some locations due to viscous damping of the turbulence by the flame. However, in regions where the vorticity is successful in penetrating the flame, the flame is extinguished and hence the local temperature is low. Based on these global observations of the vorticity and reaction rate fields it is no surprise that the reactive phenomena can significantly influence small scale mixing.

Initially, several global features of the flow and flame structure were examined to determine whether the reaction zone is consistent with the laminar flamelet picture. Since the global results

for Model 2 are similar to that for Model 1, for sake of brevity, only the salient results for Model 1 are presented here. Further details may be found in [10]. The stoichiometric surface ($Z_{St} = 0.5$) and location of the maximum value of the reaction rate coincide. Examination of temperature and reaction rate versus Z indicates that local extinction has occurred due to the existence of both large and negligible values of those quantities at the stocihiometric surface. The scalar dissipation rate χ was also found to peak at $Z = Z_{St}$ [10], and furthermore correlated well with the tangential strain rate. Therefore, the extinction pockets in Fig. 2 are a result of large tangential strain rates in the plane of the flame due to complicated vortical interactions. These global observations are consistent with the laminar flamelet picture. However, a detailed examination of the data suggests that Z and χ are not statistically independent as is assumed by the flamelet model. Furthermore, it was found (see [10]) that in regions where the strain rate is large, the flame tends to have zero mean curvature, and thus one–dimensional laminar flamelets are probably a reasonable model; however, in regions where the strain rate is low or moderate, curvature effects may need to be taken into consideration. To summarize these observations, global statistics from the DNS results suggest that the laminar flamelet approach to turbulent non– premixed combustion is a good model with the limitations that the statistical dependence between Z and χ and the influence of flame curvature need to be considered. In the next section, direct comparisons between turbulent flame statistics and laminar flame calculations are made to further evaluate the flamelet approach and its effect on the prediction of intermediate species concentrations.

Comparison between turbulent and laminar flames

Based on their studies of one–dimensional, transient diffusion flames, Maußet al. [5] reported that the overshoot of the intermediate concentrations observed in experiments may be attributed to a transient effect in which local extinction followed by reignition occurs. However, Barlow and Chen [6] pointed out that the overshoot has been observed in experiments at low enough Reynolds number at which the probability of local extinction is very low. Indeed their transient strained flame calculations produced results similar to [5] even when no extinction occurred. They concluded that differential diffusion could help explain the experimental observations. Although the chemical kinetics models used in the present study are oversimplified, they provide some additional insight on the role of time– dependent strain rates on flame structure.

In a Lagrangian frame of reference the concentration of a fluid particle observed in the (Y_A, Z)

space is governed by :

$$\frac{dY_A}{dZ} = \frac{\frac{\partial}{\partial x_i}\left(\rho \mathcal{D}_A \frac{\partial Y_A}{\partial x_i}\right) + \omega_A}{\frac{\partial}{\partial x_i}\left(\rho \mathcal{D} \frac{\partial Z}{\partial x_i}\right)}, \tag{3}$$

where Y_A, $\mathcal{D}_A$, and ω_A are the mass fraction, diffusivity, and reaction rate of species A, and ρ is the mixture density. According to this equation and depending on the Damköhler number, within a turbulent flame the concentration of a fluid particle can reach all of the values located between the equilibrium and pure mixing limits. This is observed in Figs. 3a-b where for Da $\simeq$ 1 turbulence–induced mixing influences the location of both the fully burning and frozen flow points for both Models 1 and 2. Note that the stoichiometric value of the mixture fraction is $Z_{St} = 0.5$ for both models. The transient response is due to the effects of diffusion at the small scales which is affected by the turbulence modifying the instantaneous species profile and therefore the chemical activity. Also shown in the plot are steady laminar flame predictions corresponding to low (fully burning) and high (close to extinction) strain rates. Figure 4 shows a scatter plot of the intermediate mass fraction Y_I as a function of Z. Note that the peak intermediate species concentration is approximately twice that predicted by the strained laminar flame model. This result is qualitatively consistent with OH measurements by Barlow et al. [4]. The intermediate species I formed through the first step diffuses towards both species A and B. On the B side (closer to $Z = 0$), turbulent mixing occurs leading to intermediate mass fractions much higher than the laminar value. On the A side, since the intermediate is consumed by the second step, the discrepancy between the DNS data and laminar prediction is lower. A detailed examination of the databases suggests that this behavior of radical intermediates is not dependent on the appearance of regions of extinction and/or reignition indicating that the DNS results are consistent with the simplified model of Barlow and Chen [6]. However, the exact nature of the turbulence transient is much more complicated than the simple step change in the scalar dissipation rate imposed in [6].

To facilitate comparison between the laminar and turbulent results, the maximum reaction rate normal to the stoichiometric surface is computed from the DNS database after two eddy turnover times. This is presented with respect to the inverse of the scalar dissipation rate in Fig. 5a for Model 1 and in Figs. 5b-c for Model 2. The reaction rate increases with χ until a critical value is reached at which extinction occurs. Also shown in these figures are the response curves for a typical laminar flamelet obtained from the Tsuji-burner calculations. For Model 1 the critical value of $1/\chi$ is approximately 0.06 for both cases; however, the corresponding peak reaction rate for the turbulent flame is 25% higher than that for the laminar flame. Similar qualitative trends are

observed for Model 2. At the stoichiometric surface, Y_A is plotted as a function of $1/\chi$ in Figs. 6a-b for Models 1 and 2 and Y_I in Fig. 6c for Model 2. Although, Y_A for Model 1 is consistently higher than the laminar prediction for all values of χ, Model 2 data points bracket the corresponding laminar prediction. This is because the peak reaction rate occurs at $Z = Z_{St}$ for Model 1, whereas for Model 2, peak ω_1 and ω_2 occur at locations $Z < Z_{st}$ and $Z > Z_{St}$ respectively. Consequently, at $Z = Z_{St}$, Y_A values straddle the laminar prediction. This is precisely the role of the intermediate which is produced in the first step at $Z < Z_{St}$ and consumed in the second step at $Z > Z_{St}$. Note that Y_I for the turbulent case is much higher than for the steady laminar flame, consistent with the discussion related to Fig. 4.

The trends displayed in Figs. 5 and 6 suggest that, in the turbulent flame, deviations from the steady laminar flame boundary are due primarily to the unsteadiness of the strain rate caused by the turbulence and to the turbulence–enhanced mixing which convects more reactants to the reaction zone than in a strained laminar flamelet. Because of the transient information carried by the turbulence, for a given value of the strain rate, the reactive species that are carried to the reaction zone may come from points in the vicinity of the flame that correspond to a wide range of species mass fraction values. Note in Figs. 5a-c that a substantial number of flamelets exist for values of $1/\chi$ less than the laminar critical value, supporting the notion that the flamelet in a turbulent field can sustain excursions of the scalar dissipation rate above the critical laminar value. Therefore, the interaction between finite–rate chemistry and turbulence leads to a strong modification of the local response of the reaction rate compared with the laminar flamelet.

Conclusions

1 Direct numerical simulations (DNS) of a turbulent non-premixed flame and steady laminar flame calculations were performed to evaluate the various assumptions made in the flamelet approach to modelling turbulent flames.

2 Global flame statistics obtained from the DNS suggest that overall, laminar flamelets are a good representation of a turbulent non-premixed flame, provided correlation between the mixture fraction and its dissipation rate is included at low to moderate Reynolds numbers, and curvature effects in regions of intermediate strain are properly accounted for.

3 Although the chemical kinetics models incorporated in the DNS are simple, the results suggest that overshoots in the intermediate species concentration observed in experiments may

be attributed to time–dependent strain rates associated with the turbulent flow. Other mechanisms such as differential diffusion effects are currently being examined to help fully explain discrepancies between measurements and strained laminar flame predictions.

Acknowledgments

The authors have benefited from discussion with Prof. Ishwar Puri during the 1992 CTR Stanford summer program. This research was supported by the United States Department of Energy, Office of Basic Energy Sciences, Division of Chemical Sciences and by the Center for Turbulence Research at Stanford/NASA-Ames. SM acknowledges an AWU–DOE faculty fellowship that allowed him to perform part of this research at the Sandia National Laboratories in Livermore, California.

References

[1] Bilger, R. W., *Combust. Sci. Technol.* 13:155-170 (1976).

[2] Masri, A. R., Bilger, R. W., and Dibble, R.W., *Combust. Flame* 73: 261 (1988).

[3] Stårner, S.H., Bilger, R. W., Dibble, R. W. and Barlow, R. S., *Combust. Sci. Technol.* 72: 22 (1990).

[4] Barlow, R. S., Dibble, R. W., Stårner, S. H., and Bilger, R. W., *Twenty-Third Symposium (International) on Combustion*, The Combustion Institute, Pittsburgh, 1990, pp. 583-589.

[5] Mauß, F., Keller, D., and Peters, N., *Twenty-Third Symposium (International) on Combustion*, The Combustion Institute, Pittsburgh, 1990, pp. 693-698.

[6] Barlow, R. S., and Chen, J.-Y., *Twenty- -Fourth Symposium (International) on Combustion*, The Combustion Institute, Pittsburgh, 1992, pp. 231-237.

[7] Haworth, D. C., Drake, M. C., Pope, S. B., and Blint, R. J., *Twenty-Second Symposium (International) on Combustion*, The Combustion Institute, Pittsburgh, 1988, pp. 589-597.

[8] Chen, J . H., Mahalingam, S., Puri, I. K., and Vervisch, L. 1992 Effect of finite-rate chemistry and unequal Schmidt number on turbulent non-premixed flames modeled with single-step chemistry. Paper WSS/CI 92-52, Western States Section of the Combustion Institute Fall Meeting, Berkeley

[9] Chen, J . H., Mahalingam, S., Puri, I. K., and Vervisch, L. 1992 Structure of non-premixed flames modeled with two-step chemistry; Paper WSS/CI 92-51, Western States Section of the Combustion Institute Fall meeting, Berkeley

[10] Vervisch, L., Chen, J. H., Mahalingam, S., and Puri, I. K., *Ninth Symposium on Turbulent Shear Flows*, 25-3, 1993.

[11] Trouvé, A., in *Annual Research Briefs* (P. Moin and W.C. Reynolds, Eds.), CTR, Stanford U./NASA Ames, 1992.

[12] Vervisch, L., in *Annual Research Briefs* (P. Moin and W.C. Reynolds, Eds.), CTR, Stanford U./NASA Ames, 1992.

[13] Poinsot, T., and Lele, S., *J. Comput. Phys.* 101: 104-129 (1992).

[14] Dibble, R. W. Schefer, R. W.,Chen, J. Y., Hartmann, V., Kollman, W. 1986 Velocity and density measurements in a turbulent nonpremixed flame with comparison to numerical model predictions. Paper WSS/CI 86-65, Western States Section of the Combustion Institute Spring 1986 Meeting, Banff, Canada.

[15] Smooke, M. D., and Giovangigli, V., in *Reduced Kinetic Mechanisms and Asymptotic Approximations for Methane-Air Flames* (M. D. Smooke, Ed.), Springer–Verlag, 1991.

[16] Grcar, J., *TWOPNT*, Sandia National Laboratories Report No. SAND91-8230, 1991.

Figure captions

FIG. 1. Instantaneous reaction rate isosurface for Model 1 at 10% of its maximum value after 2 initial eddy turnover times, $Da = 1$, Zeldovich number = 8.0, maximum to minimum temperature ratio = 5.0, $129 \times 65 \times 65$ grid. Note the pockets of extinction.

FIG. 2. Vorticity magnitude and reaction rate isocontours (equispaced contour levels) from a 2D slice of the flow field, for $Da = 1$ The stoichiometric mixture fraction denoted by the white line through the center of the figure is overlaid on the reaction rate contours to indicate extinguished regions. Note the vorticity magnitude is near zero across the reaction zone except in extinguished regions.

FIG. 3a. Scatter plot of mass fraction Y_A versus mixture fraction Z for Model 1, $Da = 1$. Lines denote steady laminar flame predictions, for low and high strain rates. $\triangle$: DNS data; ——: low strain rate (fully burning) ; – – –: high strain rate (close to extinction).

FIG. 3b. Scatter plot of mass fraction Y_A versus mixture fraction Z for Model 2, $Da = 1$. Lines denote steady laminar flame predictions, for low and high strain rates. $\triangle$: DNS data; ——: low strain rate (fully burning) ; – – –: high strain rate (close to extinction).

FIG. 4. Scatter plot of intermediate species mass fraction Y_I versus mixture fraction Z for Model 2, $Da = 1$. Lines denote steady laminar flame predictions, for low and high strain rates. $\triangle$: DNS data; ——: low strain rate (fully burning) ; – – –: high strain rate (close to extinction).

FIG. 5a. Distribution of maximum reaction rate ω (evaluated along local flame normal) with respect to inverse scalar dissipation rate for Model 1, $Da = 1$. Solid line denotes steady laminar flame prediction.

FIG. 5b. Distribution of maximum reaction rate ω_1 for first step (evaluated along local flame normal) with respect to inverse scalar dissipation rate for Model 2, $Da = 1$, Zeldovich number for step 1 = 8.0. Solid line denotes steady laminar flame prediction.

FIG. 5c. Distribution of maximum reaction rate ω_2 for second step (evaluated along local flame normal) with respect to inverse scalar dissipation rate for Model 2, Da = 1, Zeldovich number for step 2 = 2.0. Solid line denotes steady laminar flame prediction.

FIG. 6a. Distribution of Y_A at stoichiometric surface with respect to inverse scalar dissipation rate for Model 1, $Da = 1$. Solid line denotes steady laminar flame prediction.

FIG. 6b. Distribution of Y_A at stoichiometric surface with respect to inverse scalar dissipation rate for Model 2, $Da = 1$. Solid line denotes steady laminar flame prediction.

FIG. 6c. Distribution of intermediate species mass fraction Y_I at stoichiometric surface with respect to inverse scalar dissipation rate for Model 1, $Da = 1$. Solid line denotes steady laminar flame prediction.

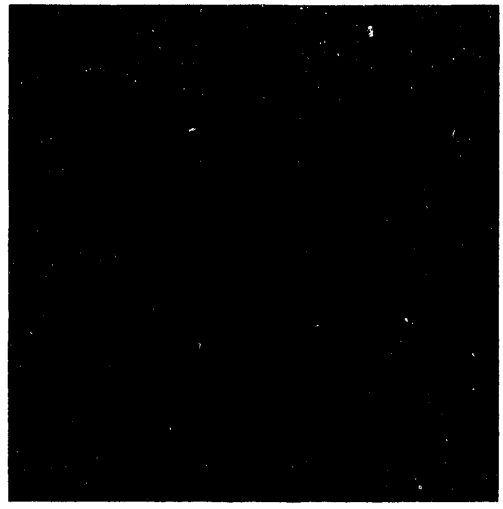

FIG. 1. Instantaneous reaction rate isosurface for Model 1 at 10% of its maximum value after 2 initial eddy turnover times, $Da = 1$, Zeldovich number = 8.0, maximum to minimum temperature ratio = 5.0, $129 \times 65 \times 65$ grid. Note the pockets of extinction.

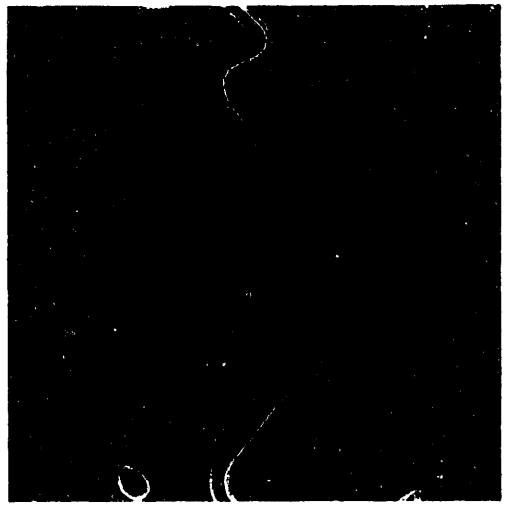

FIG. 2. Vorticity magnitude and reaction rate isocontours (equispaced contour levels) from a 2D slice of the flow field, for $Da = 1$ The stoichiometric mixture fraction denoted by the white line through the center of the figure is overlaid on the reaction rate contours to indicate extinguished regions. Note the vorticity magnitude is near zero across the reaction zone except in extinguished regions.

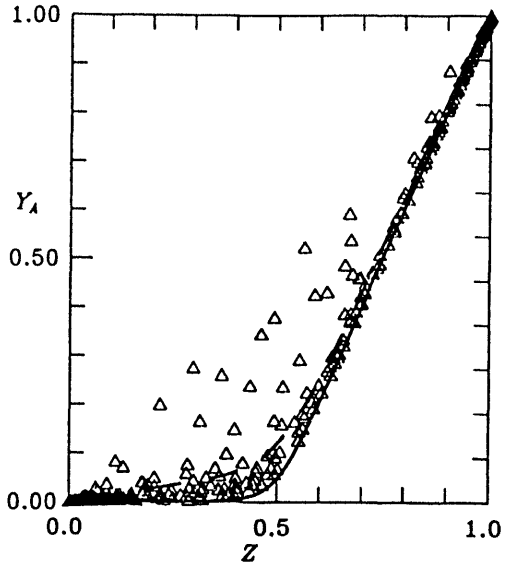

FIG. 3a. Scatter plot of mass fraction Y_A versus mixture fraction Z for Model 1, $Da = 1$. Lines denote steady laminar flame predictions, for low and high strain rates. $\triangle$: DNS data; ——: low strain rate (fully burning) ; – – –: high strain rate (close to extinction).

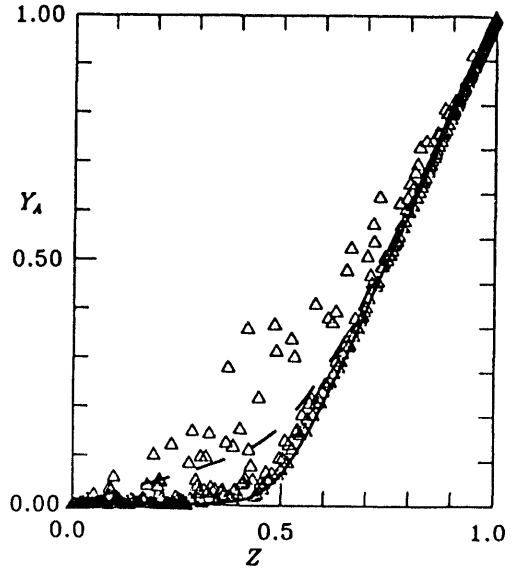

FIG. 3b. Scatter plot of mass fraction Y_A versus mixture fraction Z for Model 2, $Da = 1$. Lines denote steady laminar flame predictions, for low and high strain rates. $\triangle$: DNS data; ——: low strain rate (fully burning) ; – – –: high strain rate (close to extinction).

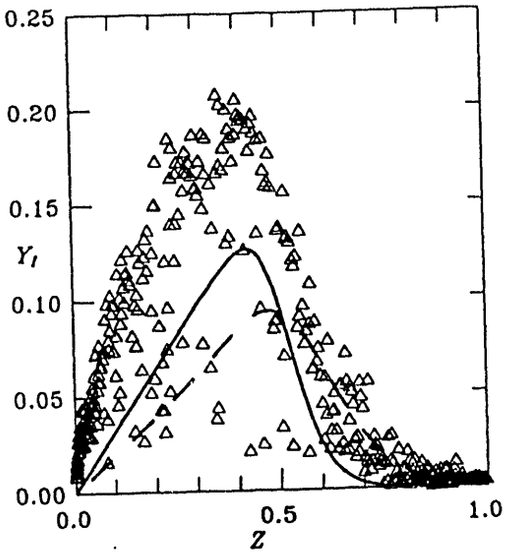

FIG. 4. Scatter plot of intermediate species mass fraction Y_I versus mixture fraction Z for Model 2, $Da = 1$. Lines denote steady laminar flame predictions, for low and high strain rates. $\triangle$: DNS data; ——: low strain rate (fully burning) ; – – –: high strain rate (close to extinction).

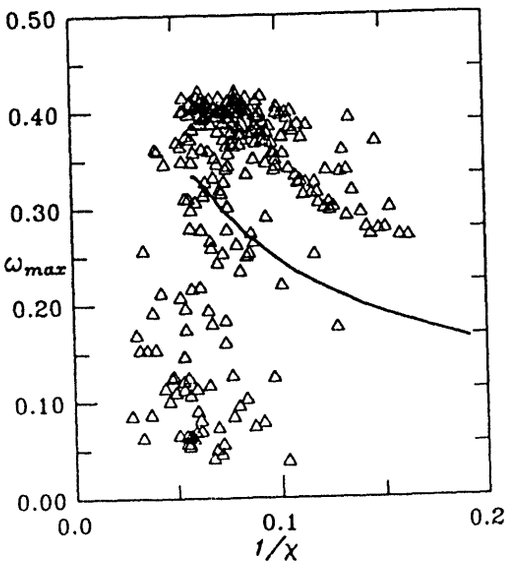

FIG. 5a. Distribution of maximum reaction rate ω (evaluated along local flame normal) with respect to inverse scalar dissipation rate for Model 1, $Da = 1$. Solid line denotes steady laminar flame prediction.

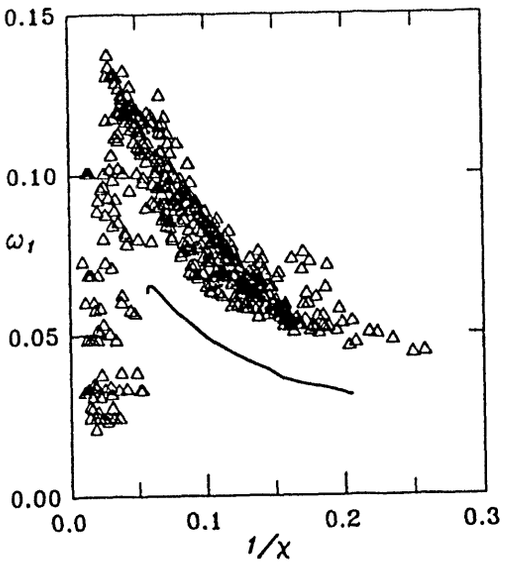

FIG. 5b. Distribution of maximum reaction rate ω_1 for first step (evaluated along local flame normal) with respect to inverse scalar dissipation rate for Model 2, Da = 1, Zeldovich number for step 1 = 8.0. Solid line denotes steady laminar flame prediction.

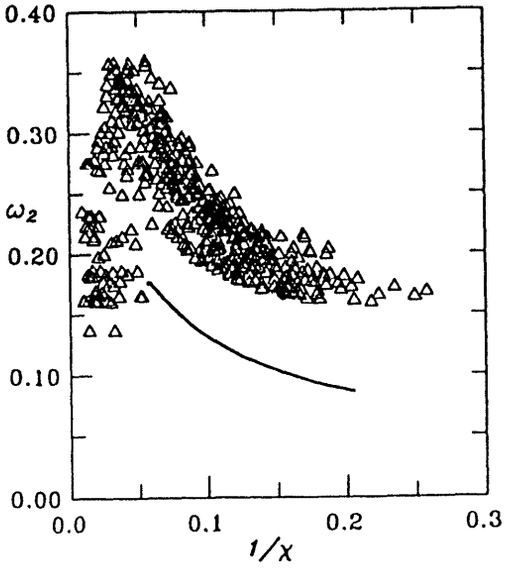

FIG. 5c. Distribution of maximum reaction rate ω_2 for second step (evaluated along local flame normal) with respect to inverse scalar dissipation rate for Model 2, Da = 1, Zeldovich number for step 2 = 2.0. Solid line denotes steady laminar flame prediction.

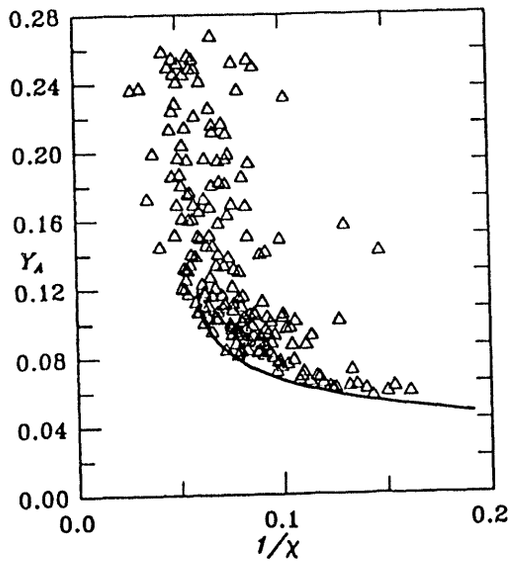

FIG. 6a. Distribution of Y_A at stoichiometric surface with respect to inverse scalar dissipation rate for Model 1, $Da = 1$. Solid line denotes steady laminar flame prediction.

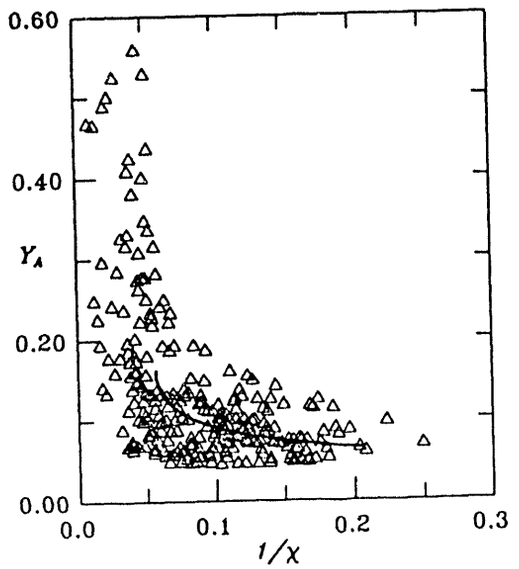

FIG. 6b. Distribution of Y_A at stoichiometric surface with respect to inverse scalar dissipation rate for Model 2, $Da = 1$. Solid line denotes steady laminar flame prediction.

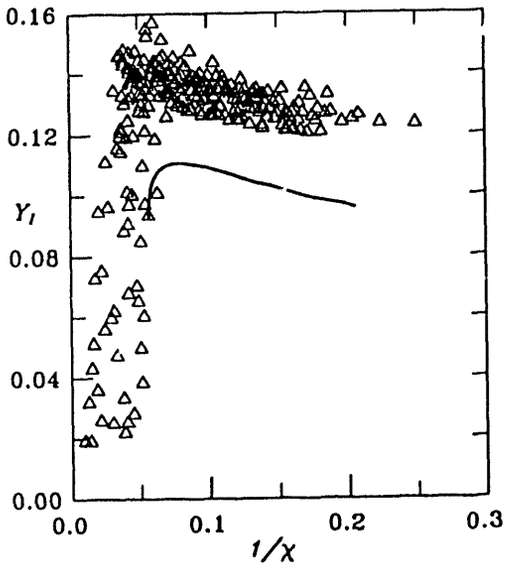

FIG. 6c. Distribution of intermediate species mass fraction Y_I at stoichiometric surface with respect to inverse scalar dissipation rate for Model 1, $Da = 1$. Solid line denotes steady laminar flame prediction.

DATE

FILMED

7/7/94

END